The Production & Analyzing Scramjets On Waverider-Derived Hypersonic Vehicle Configurations

Frederick. Ferguson,[*] Haile Lindsay[†] and Hydar Apdin[‡]
Center for Aerospace Research
North Carolina A&T State University
Greensboro, NC, 27411

This paper describes the design and analysis of scramjets integrated onto waverider-derived hypersonic vehicle configurations. The hypersonic vehicle configurations of interest to this study are derived from prescribed Two-Dimensional shock waves. Through the coupled use of the exact solutions of shock waves in an ideal gas, and the exact representations of planar geometric shapes, a series of elementary configurations are pieced together to form completed vehicle configurations. In addition, the design methodology followed in this analysis is flexible enough to allow for the aerodynamic evaluation of the resulting aircraft. Further, the design process is accomplished through the use of specially developed subroutines, to manipulate and piece elementary configurations into a system. The elementary configurations of interest are the caret and star shaped waveriders; along with waverider-derived fore-bodies, scramjets and nozzles. However, the focus of this paper is on the integration and analysis of scramjets onto the resulting aircraft. As part of this effort a FORTRAN code was developed. The code is constructed in a very efficient manner, which allows for the design and analysis of a wide class of hypersonic systems, with an option to optimize the vehicle shape and aero-thermodymanic characteristics at the designer's request. There are two important innovations to this design concept. Firstly, a reliable engineering approach is developed to integrate and analyze the geometric characteristics of the scramjet duct. This concept is based on the coupled solution of the one-dimensional conservation of mass, momentum and energy equations with heat addition, combustion and friction. Secondly, a creative engineering strategy is applied during the construction of minimum length nozzles. This paper seeks to document this design methodology, and describes in detail the integration and analysis of the scramjets as they relate to the overall hypersonic vehicle construction process. Finally, the vehicle design parameters are manipulated to generate hypersonic configurations with superior aerodynamic characteristics.

Nomenclature

α	=	angle of attack
β	=	shock wave angle
C_f	=	skin friction coefficient
C_p	=	pressure coefficient
D	=	Drag, force component parallel to the freestream velocity
γ	=	specific heats ratio

[*]Professor & Director, Center for Aerospace Research, and AIAA Senior Member.
[†]Graduate Student, Mechanical Engineering Department, and AIAA Student Member.
[‡]Graduate Student, Mechanical Engineering Department, 1601 East Market Street, Greensboro, NC 27411, and AIAA Student Member.

h = flight altitude
L = Lift, force component perpendicular to the freestream velocity
M = Mach number
μ = Mach angle
θ = wedge angle
p = pressure
u = velocity component parallel to the freestream velocity
S = Surface area
τ = shear stress
T = temperature
v = velocity component perpendicular to the freestream velocity
V = Volume

I. Introduction

IT is becoming increasingly clear that the US space program is facing a growing challenge to its global leadership position. Current launch costs are staggering, and unless reduced, these costs will continue to consume enormous resources. If fact, access to space is the most expensive item in current space program, so much so, that as a single item it continues to reduce potential achievements in space science, exploration and commerce. In response this current challenges, the center for Aerospace at North Carolina A&T State University is focusing on technologies that may lead to the development of airbreathing propulsion launch vehicles that can potentially reduced the cost of space access by a factor of 100 or more.

As such, the main objective for this research is to develop hypersonic airbreathing propulsion technologies that have the potential to provide the requirements needed to construct a wide range of vehicles that can access space at will and for a wide set of missions. In this study, an innovative engineering design approach that can provide possible baseline configurations for hypersonic airplanes, launch vehicles, and missile systems, is explored. A typical hypersonic configuration of interest to this analysis is illustrated in Figure 1. Of course, such a concept still awaits certain technological growth in material science and structures, scramjet propulsion systems, high-speed controls and vehicle systems integration. Currently, the best candidate in terms of practicality and efficiency for the hypersonic flight envelope is the waverider configuration. In the past, the waverider configuration was always thought of as a simple configuration; be it one upon which a scramjet and a nozzle after body can be easily integrated. However, only limited studies were dedicated to the actual integration of these supporting subsystems unto the main frame. The intension of this paper is to extend the waverider design concept to that of constructing a complete vehicle, which includes the fore-body, nozzle, scramjet propulsion system and wings.

Fig. 1. Hypersonic Missile Configuration

II. Design Approach

The basic approach to the effective design of waverider configurations comes mainly from the exact solution of the oblique shock-wave theory. To understand this concept, refer to Fig. 2. Consider a shockwave in a supersonic flow that is induced by the wedge, *ABC*. As indicated in Fig. 1, in the case of an inverse design approach, for a given Mach number, *M*, and for a given oblique shock wave angle, β, there is a corresponding wedge deflection angle, θ, which decides the basic geometry of the wedge. In addition, for any point, *A*, on the shockwave, for the purposes of this analysis, two lines emanate down stream, namely, line *AB*, a free stream streamline from which the upper

vehicle surface will be carved and line *AC*, from which the lower vehicle surface is carved. A typical waverider is derived from these two surfaces. Using this approach, each point lying on a leading edge curve that lies on the shock wave can contribute to the construction of the resulting waverider geometry. This concept is illustrated in Fig. 2 in the case of a wedge. This design concept is not limited to the wedge configuration. In fact, an entire vehicle can be generated using this technique.

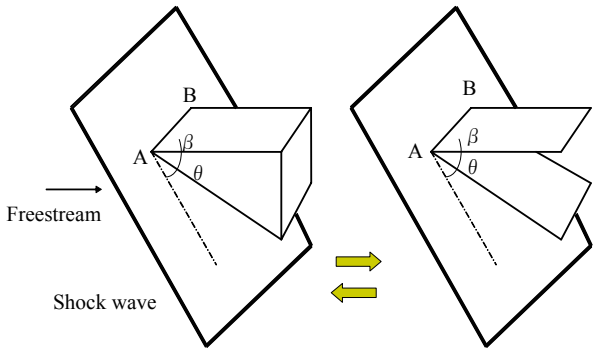

Fig. 2. 2D Waverider Design

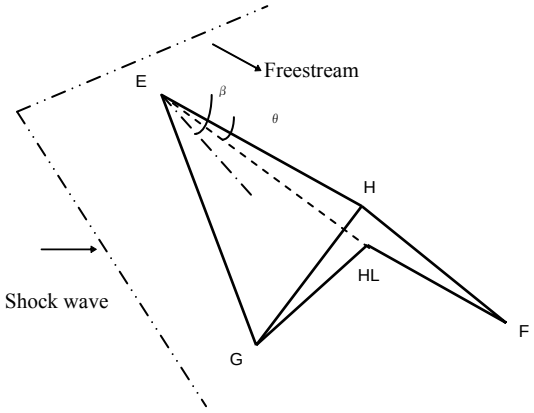

Fig. 3. A Caret Shaped Waverider

II.A. Basic Plane Generation

In general, a waverider configuration derived from 2-D shocks is composed of intersecting planes. In this analysis, the planes and lines of interest are described in the Cartesian system of coordinates, *X*, *Y* and *Z*. For example a typical plane in Cartesian coordinates is defined by the equation:

$$Ax + By + Cz + D = 0 \tag{1}$$

where *A*, *B*, *C* and *D* are constants that control the nature of the surface. A second geometric entity of interest to this study is the straight line. The equation of a line can be obtained from the unique solution obtained from the solution of two intersecting planes;

$$\begin{cases} A_1 x + B_1 y + C_1 z + D_1 = 0 \\ A_2 x + B_2 y + C_2 z + D_2 = 0 \end{cases} \tag{2}$$

Another geometric tool of interest to this analysis is the definition of a straight line through the use of the following equation:

$$\frac{(x - x_0)}{m} = \frac{(y - y_0)}{n} = \frac{(z - z_0)}{p} \tag{3}$$

where *m*, *n* and *p* are non-zero constants and (x_0, y_0, z_0) represents an arbitrary point of interest on the line. Using these definitions, a typical surface can be readily projected onto any of the three Cartesian planes, namely, *YZ*, *XZ* and *XY*. Based on the geometric principles underlining equations (1) through (3) and their derivations, a group of subroutines were developed in FORTRAN. These routines are programmed to handle the waverider design process, by generating basic planes and lines as required.

II.B. Hypersonic Forebody Generation

A typical Caret shaped waverider, illustrated in Fig. 3, is generated using the principles described earlier. In this case of a caret shaped waverider the shock wave is prescribed along with the leading edge lines, namely, *EF* and *EG*. Next, the equation for the line *EH* is prescribed using the free stream information. The point, *HL*, can be calculated through the use of the shock wave relations. Once these basic line equations are obtained the appropriate surfaces, *EHG*, *EHLG*, *EFF* and *EEFHL* are constructed through the appropriate use of the subroutine

threepointsplane. It is of interest to note that the resulting caret waverider is constructed such that it induces the prescribed shock wave. This concept was demonstrated in Ref. 1-4.

This section discusses an innovative approach to the generation of a waverider derived forebody that can be used to prepare the hypersonic flow for scramjet processing. For instance, Fig. 4 illustrates the shape of a hypersonic forebody that was constructed using this design philosophy. Splitting the caret waverider, which is illustrated in Fig. 3, at line EH and adding an appropriate wedge in between can lead to the construct of this idealized forebody configuration.

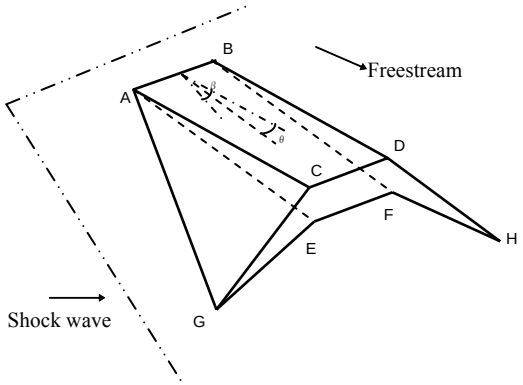

Fig. 4. A Hypersonic Forebody

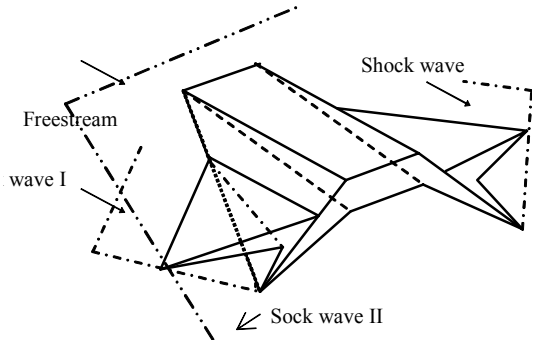

Fig. 5. An Inlet Waverider

Star-shaped waveriders are constructed from the basic caret shape, shown in Fig. 3. One caret waverider attached to another in an appropriate manner can form a star-shaped waverider. In this case, two separate shockwaves are required. The multiple uses of shockwaves as required by of the star-shaped waveriders provide great flexibility and versatility that are very important to aircraft designers. In fact, this capability is exploited in Ref. 4, to expand the waverider design space and to conduct scramjet-forebody integration studies. A hypersonic vehicle configuration with waverider derived wings is shown in Fig. 5. It is composed of an inlet as main body and two star-shaped geometries as wings. A total of three shockwaves are attached to this vehicle. Besides the added lift, the wings provide more volume to the entire vehicle.

II.C. Scramjet Combustor Design

The combustor design can follow either the concept of a constant area or variable area duct. The inlet plane to the scramjet combustor is the same as the outlet plane of the forebody, however, the exit area can be created by the designer. The length of the duct is based on the design conditions appropriate for user's prescribed scramjet model. A typical combustor generated by this design process is illustrated in Fig. 6.

At the end of the hypersonic forebody design phase, not only is the shape of the inlet to the scramjet combustor known, but also the mass flow rate. In addition, for effective combustor designs, it is required that the mass flow ejected from the scramjet does so under choked conditions. To satisfy these requirements, certain assumptions are made. First and foremost, effective mixing is assumed such that completed combustion occurs within the combustor and just prior to the scramjet exit plane. This process can be described by the empirical expression given in Ref. 2,

$$\tau_R = 325\, p^{-1.6}\, e^{-0.8 T_0 / 1000} \tag{4}$$

where, τ_R represents the inverse of the reaction time, and p the average pressure, and τ_0, the total temperature within the scramjet. It is also of interest to note that the combustion time will determine the length of the combustor, since this length can be expressed simply as

$$L_{scramjet} = \frac{V_{avg}}{1/t} = \left(\frac{M_{in} + M_{out}}{2}\right)\frac{\sqrt{\gamma R T_{in}}}{\tau_R} \tag{5}$$

where γ and R are the ratio of the specific heats and the universal gas constant, and M_{in}, M_{out}, and T_{in} represents the average Mach numbers and temperature entering and leaving the scramjet. After rearranging equations (4) and (5), and manipulating a few constants the following equation is obtained

$$\left(\frac{L}{H}\right)_{scramjet} = \frac{C\left(M_{ref}+1\right)\sqrt{\gamma R T_{ref}}}{p_{ref}^{-1.6}\, e^{-0.8\, T_{0,ref}/1000}} \tag{6}$$

However, in equation (12), the quantities with the subscripts, 'ref', such as, M_{ref} , T_{ref} , p_{ref} , and $T_{0,ref}$, represent average thermodynamic parameters at the entrance of the combustor, and the symbol C represents a const value. The scramjet length is non dimensionalized with respects to the combustor height, *H*. As illustrated in equation (12), $L_{scramjet}$ is highly dependent on the nature of the thermodynamic processes within the combustor.

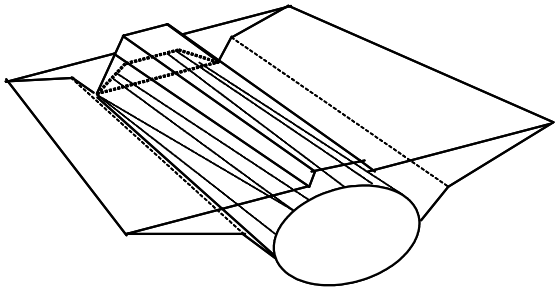

Fig. 6: A Typical Combustor Design

II.D. Nozzle Design

The method of characteristics (MOC) is used to define the scramjet nozzle. Here again, the inlet plane to the nozzle is the same as the combustor's exit plane. However at this plane the conditions of choked quasi-1D flow is assumed. In addition, this design analysis requires that the exit plane of the nozzle has a Mach number equals to that of the freestream. With these design conditions it can easily be shown that the nozzle shape, *y = y(x)*, can be constructed in accordance with the following equation:

$$\frac{dy}{dx} = \tan\left(\theta \pm \mu\right) \tag{7}$$

where the θ and μ, are functions of the local Mach number within the nozzle. Further, in this analysis based on the MOC, θ and μ can be defined as follows:

$$\theta = \tan^{-1}(v/u) \tag{8}$$

$$\mu = \sin^{-1}(1/M) \tag{9}$$

and where *u* and *v* are velocity components in *X* and *Y* direction, respectively.

It is of interest to note that the nozzle contours generated by this method is very sensitive to changes in the free stream Mach numbers. It was found that for high mach numbers, the nozzle dimensions were not practicable. In this analysis, an engineering design approach was created to correct this problem,. This approach is based on the knowledge that the typical behavior of the nozzle contour is to first rapidly increase over the first 25% of its length and slightly and slowly tapered on to zero over the remaining75%. An design parameter based on the nozzle slope, $\delta, (0 \le \delta \le 0.2)$, was introduced.

II.E. Vehicle Integration and Leading Edge Bluntness

One of the keys of the success of an airbreathing hypersonic vehicle is the effective integration of the airbreathing engine with the airframe. A successfully integrated engine/airframe system must yield a high thrust margin while maintaining a high lift to drag ratio and a high volumetric efficiency while maintaining a reasonable balance between the forebody and nozzle forces. There are also many aerothermodynamic parameters which affect the overall performance of the airbreathing hypersonic vehicle. For example a uniform flow field in the combustor is essential for effective combustion to occur. Since the vehicle forebody form the flow field provided to the engine it must be designed in a manner that will satisfy this condition. The location of the engine is also important. The engine must be in a location that it can capture the compressed flow provided by the forebody. For flight Mach

number above five, the temperatures on sharp leading edges exceed the thermal limits for most materials. As such, for any considerations in the hypersonic flight regime only blunt leading edges are practical. In general, the leading edge (LE) bluntness radius is chosen to be about 5-6% of the forebody's overall length. These concerns are all taken into consideration as the individual components of the vehicle is pieced together.

Consider a typical leading edge location as illustrated in Figure 8 The radius, R, (where R = CD) of the required arc and the location of its center, C, and can be evaluated based of the following equations:

$$R = BD \,/\, Cos\,\theta \tag{10}$$

where the length BD can be readily obtained and the angle, θ, calculated from the expression,

$$\theta = a\tan\left(\frac{Y_D - Y_A}{X_D - X_A}\right) \tag{11}$$

In addition, the coordinates, X_A, X_D, Y_A, and Y_D are known. Similarly, the coordinates of the point C, X_C and Y_C, are evaluated as follows:

$$\begin{cases} X_C = R\,Sin\,\theta \;+\; AB \\ Y_C = 0 \end{cases} \tag{12}$$

In this analysis, the construction of the arc for leading edge bluntness is constructed through the use of n number of points. At each point the coordinated x_i and y_i, i = 1, n, are evaluated as follows:

$$\begin{cases} x_i = x_c - R\,Cos\,(\alpha_i) \\ y_i = R\,Sin\,(\alpha_i) \end{cases} \tag{14}$$

Where the parameter, α_i, is calculated through the use of the expression, $\alpha_i = i\alpha/(n-1)$.

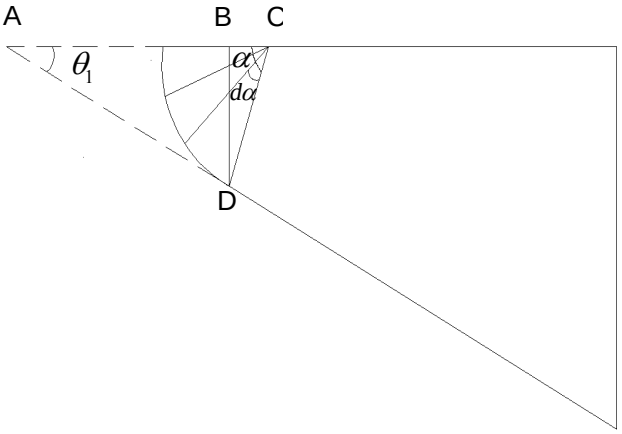

Fig. 7: Leading Edge Bluntness Design

So far, the geometry discussed in this paper is of a 2D nature, with surface pieced together from 2D planes. At this stage a typical designer has many options in terms of closing generating a final shape. A simple option is to proceed to the vehicle closure process with only bluntness in the leading edges. Another option is to introduce generalized smoothing within the confines of the 2D configuration to preserve the aerodynamic characteristics of the vehicle while improving its localized aerothermodynamics properties. This has been accomplished by using the following equation to generate smooth surfaces;

$$\begin{aligned} y(i,j) &= y_C(i) + R(i)\cos(\alpha(j)) \\ z(i,j) &= R(i)\left(1 - \varepsilon\sqrt{\sin(\alpha(j))}\right)\sin(\alpha(j)) \end{aligned} \tag{15}$$

where $y_C(i)$ represents the side center and $R(i)$ is half of the distance between the top surface and the bottom surface at a certain station from the leading edge. In this study, the symbol, ε, is considered as the vehicle side-surface design parameter. Typical hypersonic vehicle configurations generated by this code are illustrated in Figs. 8 and 9.

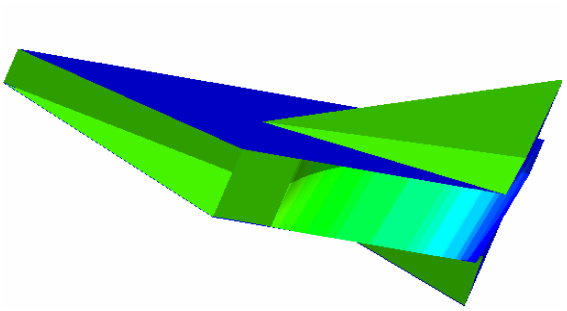

Fig. 8. A typical constant area combustor

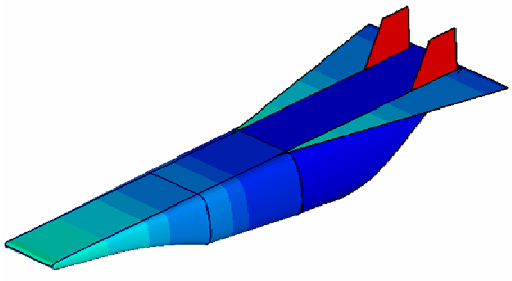

Fig. 9. Hypersonic Vehicle with Blunted Les

III. Aerodynamic Forces Evaluation

The aerodynamic analysis of the generated hypersonic vehicle was conducted through the use of two separate but complementary analyses procedures. Viscous and inviscid analyses were conducted separately, since the total corresponding force acting on the vehicle can be expressed as follows,

$$\overline{F} = \overline{F}\left(\mathrm{P}, \tau\right) \tag{16}$$

where P is the pressure and τ is the shear stress . In fact, the aerodynamic force is obtained through the integration of the local pressure and shear stress over the vehicle's surface through the use of the expression,

$$\overline{F} = \iint_{S} \mathrm{f}\left(\mathrm{P}, \tau\right) d\overline{S} \tag{17}$$

where dS defines an infinitesimal surface element. The force x-components contribute to the vehicle's total drag and the y-components contribute to vehicle's total lift. However, the force component in z-direction is neglected in this study due to the fact that the forces acting in opposite direction have the same magnitude.

The lift and drag forces acting on the hypersonic vehicle configuration can be estimated by analyzing the forces due to pressure and shear stress as illustrated in Figure 10. In fact, the expression used to calculate the lift and drag forces in this particular study are as follows:

$$L = P_{avg} \,.\, Area_{plan} + \tau_{avg} \,.\, Area_{base} \tag{18}$$

$$D = P_{avg} \,.\, Area_{base} + \tau_{avg} \,.\, Area_{plan} \tag{19}$$

where P_{avg} and τ_{avg} represent the average aerodynamic and viscous forces due to the pressure and shear stress acting on the base and plan form projected surfaces of the aircraft, respectively. Finally, the lift and drag coefficients are evaluated by using the following expressions,

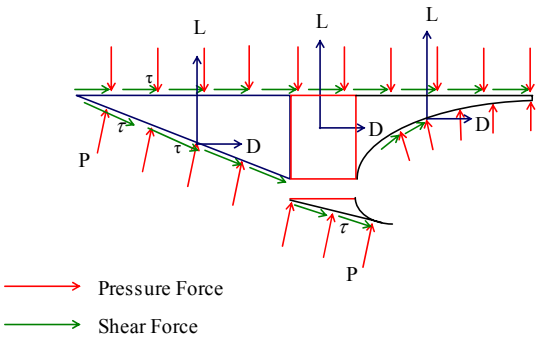

Fig. 10: Aerothermodynamic Analysis

$$C_L = \frac{L}{q_\infty S} \tag{20}$$

$$C_D = \frac{D}{q_\infty S} \tag{21}$$

where q_∞ is the freestream dynamic pressure.

III.A. Average Pressure Estimation

An estimation of the local pressure distribution, $P = P_{i,j}; (1 \le i \le II, 1 \le j \le JJ)$, on the hypersonic vehicle is conducted through the use of the expression,

$$P = P_\infty + C_p \, q_\infty \tag{22}$$

where the symbols, q_∞ and C_p represents the free stream dynamic pressure and the pressure coefficient. In this analysis, C_p can be calculated by the modified Newtonian formulation, (Ref .3)

$$C_p = C_{p_{\max}} \sin^2 \theta \tag{23}$$

where the maximum value of the pressure coefficient, $C_{p_{\max}}$ is determined by using the following expression,

$$\mathrm{Cp}_{\max} = \frac{2}{\gamma \, \mathrm{M}_\infty^2} \left\{ \left[\frac{(\gamma+1)^2 \, \mathrm{M}_\infty^2}{4\gamma \, \mathrm{M}_\infty^2 - 2(\gamma+1)} \right]^{\gamma/(\gamma-1)} \left[\frac{1 - \gamma + 2\gamma \, \mathrm{M}_\infty^2}{\gamma+1} \right] - 1 \right\} \tag{24}$$

Finally, the average pressure is determined as follows:

$$\mathrm{P}_{avg} = \frac{\sum_{i,j} P_{i,j}}{number \; of \; grid \; points} \tag{25}$$

III.B. Average Shear Stress Estimation

The expression for the local skin friction coefficient, c_f, for the laminar and turbulent flows are given by Ref. 4 in the form:

$$c_f = \begin{cases} \dfrac{0.664}{\sqrt{\mathrm{Re}_x}} \left[0.45 + 0.55 \dfrac{T_w}{T_\infty} + 0.09(\gamma-1)\sqrt{\mathrm{Pr}} \, M_e^2 \right]^{-\frac{1-\omega}{2}}; & Lam \quad Flow \\ \dfrac{0.0592}{\mathrm{Re}_x^{0.2}} \left(1.0 + \dfrac{(\gamma-1)}{2} \mathrm{Pr}^{1/3} \, M_e^2 \right)^{-0.55} \left(\dfrac{T_w}{T_e} \right)^{-0.21}; & Turb \quad Flows \end{cases} \tag{26}$$

where Re_x is the local Reynolds number and ω is the exponent for the viscosity variation. Using the expressions in (13) and (14) the appropriate local shear stress, τ_w, $\tau_w = \tau_{i,j}; (1 \le i \le II, 1 \le j \le JJ)$ quantity; laminar or turbulent, can be evaluated as follows:

$$\tau_w = c_f \, q_e \tag{27}$$

In the present waverider analysis, the values for $\gamma, \omega,$ and Pr are chosen as follows[3-4,7-10]:

$$\begin{aligned} &\gamma = 1.4 \\ &\omega = 0.75 \\ &\mathrm{Pr} = \begin{cases} 0.71 & \text{laminar flow} \\ 0.89 & \text{turbulent flow} \end{cases} \end{aligned} \tag{28}$$

The boundary layer transition the relationship given by[3-4,7-10]:

$$\log_{10} \mathrm{Re}_{z,tr} = 6.421 \, e^{(1.209 * 10^{-4} M_e^{2.641})} \tag{29}$$

Finally, the average shear stress on the vehicle surface is evaluated as follows:

$$\tau_{avg} = \frac{\sum_{i,j} \tau_{i,j}}{number\ of\ grid\ points} \tag{30}$$

IV. Hypersonic Vehicle Flow Path Analysis

While the concept behind the scramjet is very simple, the practical ramifications of hypersonic travel are quite formidable. A couple of the challenges are supersonic fuel-air mixing, and heat dissipation both from the air friction and the internal combustion. Consequently, the flow path of the incoming air needs to be extremely precise to minimize hot spots. By far the biggest challenges the scramjet face are those arising from the intense operational temperatures. Since the air entering the engine is already heated by friction with the engine walls, combustion chamber temperatures would exceed 5000 degrees Fahrenheit, if left unchecked. At these temperatures most metals melt, and air and fuel become ionized so that the physics of their behavior becomes unpredictable. Even when the heat is dissipated efficiently, the structural strength of most metals declines dramatically at the operating temperatures, so a different type of heat conducting material has to be used. Composites are the material of choice, but only after extended research and testing can a suitable material be developed. In practice, aircraft weight has to be kept to a minimum, while maintaining structural strength and rigidity to dampen the tremendous vibrations that can occur at hypersonic speeds. Due to these and other inherent design complexities, progress in the field of scramjet research has been extremely slow. However, due to recent findings of Russian, and French scramjet experiments, the successful experimental scramjet flights conducted by the Australian and Americans, these is renewed interest in this area of propulsion.

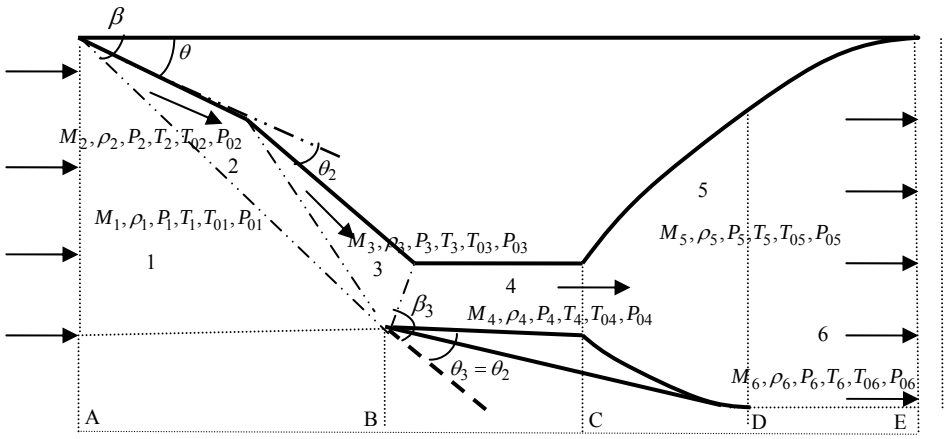

Fig. 11: Hypersonic vehicle flow path analysis

IV.A. Oblique Shock Wave Calculations

This section briefly describes the basic equations needed for the hypersonic vehicle flow path analysis illustrated through the use of a control volume in Figure 11. The hypersonic vehicle flow path analysis involves the evaluation of the flow field properties in the six different regions that makes up the flow path control volume. Further, each separated with the virtual surfaces, AA', BB', CC', DD' and EE'. Evaluation of the flow fields in regions 1 through 4 are relatively straight forward and can be easily accomplished through the use of equations (31) through (38) listed in Table 1. The other oblique shock relations[6] of interest to this study are listed below:

Table 1. Equations Used in Aerodynamic Analysis

$M_{n,1} = M_1 \sin\beta$	(31)	$\frac{\rho_2}{\rho_1} = \frac{(\gamma+1)M_{n,1}^2}{2+(\gamma-1)M_{n,1}^2}$	(35)
$M_{n,2}^2 = \frac{1+[(\gamma-1)/2]M_{n,1}^2}{\gamma M_{n,1}^2-(\gamma-1)/2}$	(32)	$\frac{p_2}{p_1} = 1+\frac{2\gamma}{\gamma+1}(M_{n,1}^2-1)$	(36)
$M_2 = \frac{M_{n,2}}{\sin(\beta-\theta)}$	(33)	$\frac{T_2}{T_1} = \frac{p_2}{p_1}\frac{\rho_1}{\rho_2}$	(37)
$\frac{\rho_2}{\rho_1} = \frac{(\gamma+1)M_{n,1}^2}{2+(\gamma-1)M_{n,1}^2}$	(34)	$\frac{P_0}{P} = (1+\frac{\gamma-1}{2}M^2)^{\gamma/(\gamma-1)}$	(38)

Appropriate care must be taken during the evaluation of equations (31) through (38) as it is applied to each zone boundary; namely, *1-2, 2-3* and *3-4*. In addition, precautions must be taken as the following $\theta-\beta-Mach$ relations;

$$\tan\theta = 2\cot\beta\frac{M_1^2\sin^2\beta\ -1}{M_1^2(\gamma+\cos 2\beta)+2} \tag{39}$$

are applied.

IV.B. Scramjet Performance Analysis

At this stage it is reasonably to assume that the flow field properties at the entrance of the scramjet combustor are known. The next step is the evaluation of the average flow field properties in the scramjet, based on an ideal representation of the combustion process.

The stoichiometric fuel to air ratio, f_{st}, is the ideal upper limit for the fuel to air ratio that corresponds to complete mutual combustion of all the oxygen present in the air with all the reactants available in the fuel. The underlying assumption is that anything less would not take full advantage of the available oxygen, and anything less would waste the fuel that could not be burned. Since almost all the fuels under consideration for hypersonic flights are hydrocarbons, the general chemical equation for their complete combustion with the air available in Earth's atmosphere is given by

$$C_xH_y + \left(x+\frac{y}{4}\right)\left(O_2+\frac{79}{21}N_2\right) \rightarrow xCO_2+\frac{y}{2}H_2O+\frac{79}{21}\left(x+\frac{y}{4}\right)N_2 \tag{}$$

Using this expression, the stoichiometric fuel to air ratio, f_{st}, can be obtained in the form

$$f_{st} = \frac{36x+3y}{103(4x+y)} \tag{}$$

In this analysis, hydrogen is the scramjet fuel of choice, and it is assumed that the stoichiometric fuel to air ratio is equal to the fuel to air ratio, ($f_{st} = f$); as such, x and y take on the values of 0 and 2, yielding a value of $f_{st} = 0.0291$.

The rate at which chemical reactions make energy, $\dot{q}_{\max}$, available to the engine cycle is defined as, $\dot{q}_{\max} = f_{st}\dot{m}_{inlet}h_{PR}$, where $h_{PR} = 119,954\ kJ/Kg$ when hydrogen is used to fuel the scramjet. The quantity, $\dot{q}_{\max}$, obtained from this simplified analysis will be used in the evaluation of the energy equation later in this paper.

The 1 D mass flow equation can be written in the form,

$$\dot{m}_{ref} = A_{ref}\ p_{ref}\ M_{ref}\sqrt{\frac{\gamma}{RT_{ref}}} \tag{40}$$

where the symbols, A, represents the area of the scramjet duct, and the symbol, $\dot{m}_{inlet}$, represents the mass flow rate, $\dot{m}_{inlet}$, at the inlet or station B. In this analysis these quantities are known. The integral form of the momentum equation as applied to region 4 leads to the thrust equation in the forms;

$$T_4 = \dot{m}_B\left\{(1+f)u_c - u_B\right\} + \left(\int_B P_{C,ref}\,ds - \int_C P_{B,ref}\,ds\right) \tag{41}$$

where the symbol, T_4, $P_{D,ref}$ and $\dot{m}_D$ represents the scramjet thrust, the average pressures and the mass flow rates at virtual surfaces, B and C. A simplified analysis for 1D flow with heat addition, based on Ref. 1, gives an expression for the maximum heat flux, $\dot{q}_{\max}$, in the form,

$$\dot{q}_{\max} = c_p\ T_{ref}\frac{\left(M_{ref}^2 - 1\right)^2}{2M_{ref}^2\ (1+\gamma)} \tag{44}$$

where the symbols, c_p and $\dot{q}_{\max}$, represents the specific heat and the maximum heat flux, respectively.

A careful review of the conservation equations indicates that the following 'ref' set of flow parameters, P_{ref}, T_{ref} and ,$T_{0,ref}$ can be evaluated from the following equations:

$$\begin{aligned} T_{ref} &= \frac{2\ \dot{q}_{\max}\ (\gamma+1)\ M_{ref}}{C_p\ (M_{ref}^2 - 1)} \\ T_{0,ref} &= T_{ref}\ \left(1+\tfrac{\gamma-1}{2}\ M_{ref}^2\right) \\ P_{ref} &= \frac{\dot{m}_{inlet}\ \sqrt{\gamma\ R\ T_{ref}}}{\gamma\ A\ M_{ref}} \end{aligned} \tag{45}$$

where the only unknown is M_{ref}. Further, M_{ref} can be found by iteratively solving the 1D momentum equation for choked flow with friction in the form,

$$\left(\frac{L}{H}\right)_{scramjet} = \frac{1}{4f}\left\{\frac{1-M_{ref}^2}{\gamma M_{ref}^2} + \frac{\gamma+1}{2\gamma}\ln\left[\frac{(\gamma+1)M_{ref}^2}{2+(\gamma-1)M_{ref}^2}\right]\right\} \tag{46}$$

Having evaluated the average flow field parameter in the scramjet, all other parameters of interest to the scramjet can be evaluated including the scramjet propulsive and overall efficiencies listed as equation () and () in Table 2.

Table 2. Equations Used in Aerodynamic Analysis

Propulsive Efficiency		Overall Efficiency	
$\eta_p = \dfrac{2\left\{(1+f)\dfrac{u_c}{u_D} - 1\right\}}{\left\{(1+f)\left(\dfrac{u_c}{u_D}\right)^2 - 1\right\}}$	(32)	$\eta_O = \dfrac{Fu_B}{\dot{m}_f h_{PR}}$	(36)

IV.C. Nozzle Analysis

Similarly, the thrust generated by the control volume in zone 5, and bordered virtual surfaces C and D is evaluated as follows;

$$T_5 = \left(\int_D P_{D,ref}\, ds - \int_C P_{C,ref}\, ds \right) + \left(\dot{m}_D u_D - \dot{m}_C u_C \right) \qquad ()$$

where the symbol, T_4 , T_5 $P_{D,ref}$ and $\dot{m}_D$ represents the scramjet and nozzle thrust, the average pressures and the mass flow rates at virtual surfaces, B and D.

V. Results and Analysis

In this section the hypersonic vehicle design code is used to identify the design variables and their sensitivity with respects to the vehicle's aerodynamic performance. Lift over drag (L/D) analysis was conducted with respect to two sets of design variables; namely, the vehicle geometric properties, and the freestream Mach number. The geometric variables considered as part of this analysis are: the forebody or wedge deflection angle, θ, and the inlet to nozzle length ratio, l. The effects of the Mach number and the wedge deflection angle on the vehicle geometric properties, such as volume and wetted surface area, were also studied.

Table 2. Example of the inputs and outputs of the program

Input		**Output**	
Mach Number	5.0	Inlet Angle(θ)	20°
Altitude (H)	30 km	Surface Area	97.6 m^2
Shock Angle (β)	30°	Volume	21.6 m^3
Inlet Length (L_i)	5 m	Lift	664 kN
Inlet Width(W_i)	2 m	Lift Coefficient (C_l)	0.12
Combustor Length(L_c)	20% L_i	Drag	210 kN
Nozzle Length(L_n)	80% L_i	Drag Coefficient (C_d)	0.039
		L/D	3.2
		Average Upper Surface, c_f	3.95×10^{-4}
		Average Lower Surface, c_f	5.76×10^{-4}

V.A: Hypersonic Vehicle Performance Analysis

A typical input set used by this code, and a typical output data set generated by it are listed in Table 2. In addition, a typical hypersonic vehicle generated from the use of this data is shown in Figure 16. Figure 17 shows the surface area and volume variations for a typical hypersonic vehicle ranging from Mach numbers 3 to 10. It is notable that the surface area is not sensitive to the Mach number; this condition is favorable for the shear stress considerations. Note that the volume changes noticeably with the Mach number increasing. This is explained by the fact that for the same shock wave angle β the inlet wedge deflection angle θ increases as the Mach number increases, which in turn contributes to the volume. Figure 18 shows that the vehicle's surface area and volume varying gently within certain range of the wedge deflection angle, θ, but rapidly increase at angles greater than 25 degrees.

Further, it was found that the L/D increases linearly with the nozzle to inlet length ratio, l, but the L/D decreases rapidly with an increase in the wedge deflection angle, θ. As illustrated in Figures 19 and 20, the L/D ratio is very sensitive to the wedge deflection angle θ but varies gently relative to changes in the nozzle to inlet length ratio. This indicates that the design method is adaptive in generating vehicles with different sizes without losing too many of the benefits of achieving a higher L/D ratio.

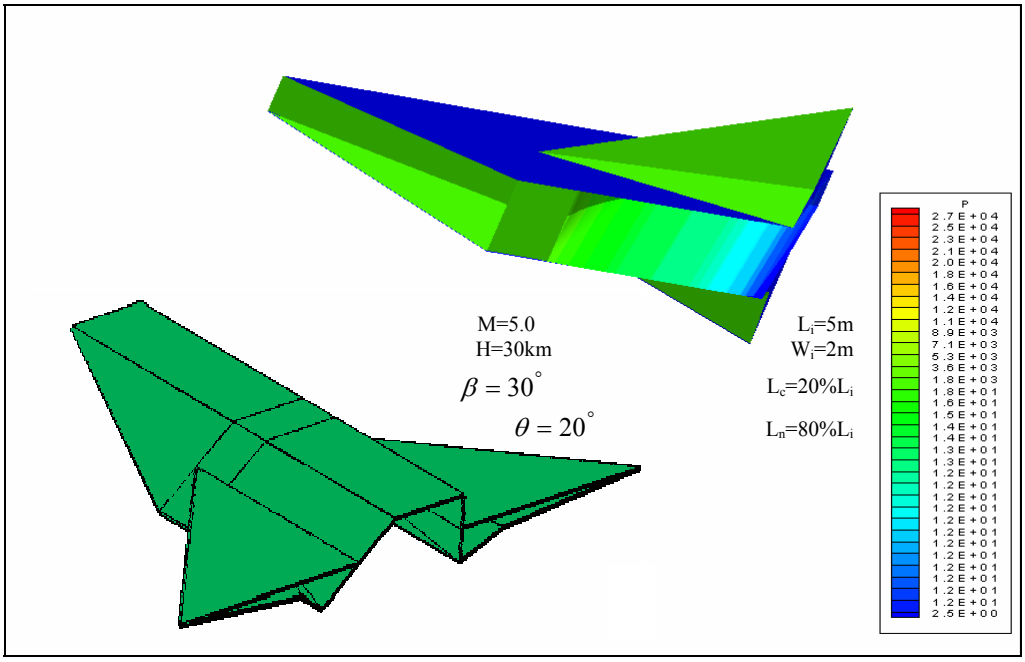

Fig. 16. Complete waverider configurations with different perspective views

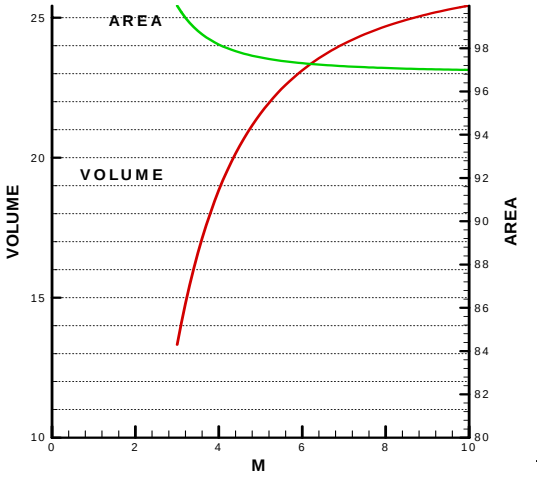

Fig. 17. Surface area and volume vs. Mach number

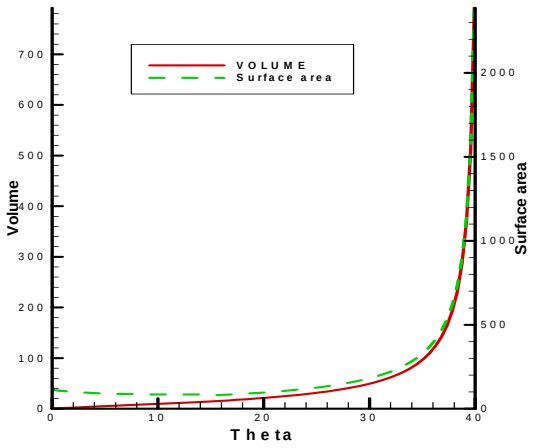

Fig. 18. Surface and volume vs. deflection angle

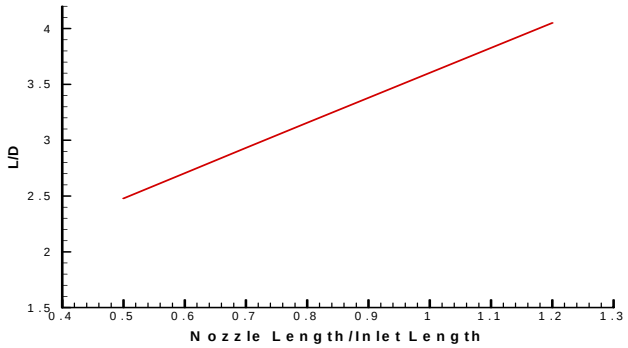

Fig. 19. L/D ratio vs. nozzle length

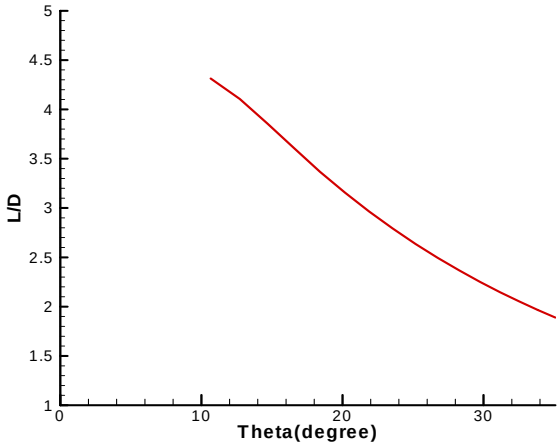

Fig. 20. L/D ratio vs. deflection angle

V.B: Hypersonic Vehicle L/D Analysis

Using the analytical capabilities of the code developed herein, a preliminary design analysis was conducted and the results tabulated in Table 3. The shaded area illustrated in Table 3, at a given row, represents the typical data set required by the waverider design code, and the L/D column represents the calculated vehicle design characteristics. Table 3 represents the collective behavior and the creative potential of the waverider design code. The performance outcome depicted in Table 3 can also be represented as design points on the Kuchemann curves illustrated in Figure 21.

Table 3. A group of optimized waverider designs

M	H (km)	Li (m)	Wi	Lc/Li	Ln/Li	β (degree)	L/D
5.0	30	5	2	0.25	1.3	18	5.17
8.0	30	7	2	0.25	0.9	16	5.51
10.0	30	7	2	0.25	0.9	16	5.41
12.0	30	7	2	0.25	0.9	16	5.35
15.0	30	7	2	0.25	0.9	18	4.90
17.0	30	7	2	0.25	1.0	18	5.16

The L/D hypersonic barrier based on actual flight test data given in Ref. 14 is represented by the following relationship:

$$\left(\frac{L}{D}\right)_{\max} = \frac{4(M+3)}{M} \tag{35}$$

Equation (35) is depicted in Figure 21 by a dashed line. However, a much closer representation of the L/D ratio for viscous optimized waverider is given in Ref. 3; the curve is also shown in Figure 21 by the solid line, which represents the correlation:

$$\left(\frac{L}{D}\right)_{\max} = \frac{6(M+2)}{M} \tag{36}$$

The L/D ratio for the hypersonic vehicles generated during this study using the arbitrary input data sets tabulated in Table 2 are illustrated as stars in Figure 21. It is of interest to note that for the vehicles constructed herein, delivers L/D performance ratios within the values predicted by equations (35) and (36), and it has a trend similar to the Kuchemann curves.

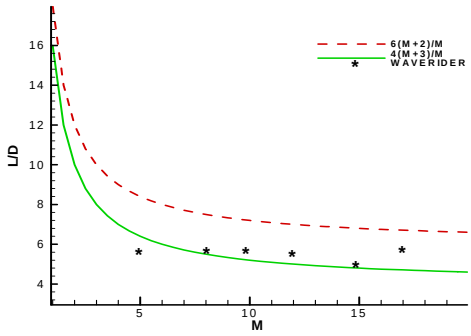

Fig. 21. L/D ratio vs. Mach Number

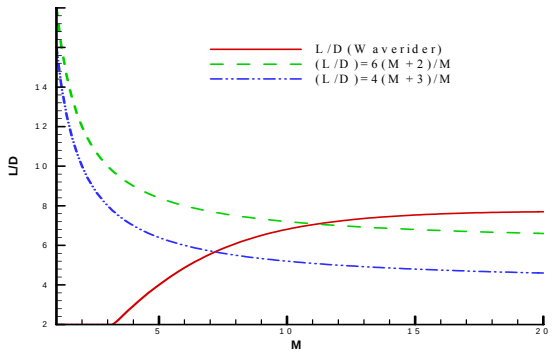

Fig.22. Optimized L/D ratio vs. Mach number.

VI. Conclusion

The design process for constructing waverider derived hypersonic vehicle is outlined, and documented in the creation of a FORTRAN based program. All subroutines used to design the various elements were explained. The methods used to evaluate the lift and drag characteristics of the vehicle are described, and their relationship to the local pressure and shear stress distributions over the vehicle surface are documented. Further, the algorithms used for the calculations of the vehicle aerodynamic performance are described in detail in this paper. In addition, the basic equations used for the evaluations of the geometric characteristic of the vehicle are also documented.

Using the newly developed program, the volume and the surface area of the hypersonic configuration, in addition to its lift and drag coefficients, and its L/D ratio, were analyzed with respects to certain design parameters. Further, the L/D ratio was studied as it relates to changes in the geometric variables. The L/D versus the Mach number behavior was compared with the Kuchemann barriers with respect idealized hypersonic configurations. The resulting L/D ratios of this waverider-derived vehicles falls within the Kuchemann barriers and produced a behaviors trend similar to that of the Kuchemann curves.

Finally, the hypersonic vehicle code was used to identify the design variables; including both aerodynamic and geometric parameters, that are most sensitivity to the overall performance of the resulting vehicle. After a careful analysis, the following design parameters were identified: Mach number, flight altitude, the ratio of the vehicle nozzle length to the inlet length, the wedge angle and the vehicle wing span. Further, it was found that once the right combination of these parameters was found at a given Mach number, the optimum L/D values were found to be very attractive. In fact, under these conditions, the resulting optimum L/D versus the Mach number curve delivered a very interesting behavior when compared to the Kucheman barriers. This result is illustrated in Figure 22.

VII. Acknowledgments

This work has been partially sponsored by the following agencies; the National Institute of Aerospace, NASA Glenn and Langley Research Centers. In addition, special appreciation is extended to the Space Vehicle Technology Institute, one of the NASA University Institutes, with joint sponsorship from the Department of Defense. Appreciation is expressed to Claudia Meyer, Mark Klemm, Isaiah Blankson and Harry Cikanek of the NASA Glenn Research Center, and to Dr. John Schmisseur and Dr. Walter Jones of the Air Force Office of Scientific Research.

VIII. References

[1]Nonweiler, T., "Aerodynamic Problems of Manned Space Vehicles," Journal of Royal Aeronautical Society, Vol. 67, Jan. 1963.

[2]Nonweiler, T., "Delta wings of Shapes Amendable to Exact Shock Wave Theory," Journal of Royal Aeronautical Society, Vol. 67, Jan. 1963.

[3]Bowcutt, Kevin G., Anderson, John D. Jr., and Capriotti, D.P., "Viscous Optimized Hypersonic Waveriders," AIAA paper 87-0272, 1987.

[4]Ferguson, F., "Expanding the Waverider Design Space Using Arbitrary Generating Flowfields", Ph.D. Dissertation, Department of Aerospace Engineering, University of Maryland, College Park, Maryland, 1993

[5]http://mathworld.wolfram.com/, Wolfram Research, Inc.
URL: http://mathworld.wolfram.com/topics/AlgebraicGeometry.html, Feb.15, 2005.

[6]John D.Anderson "Fundamentals of Aerodynamics" Third Edition, 2001, McGRAW-HILL.

[7]Young, A.D., "Modern Developments in Fluid Dynamics', Vol. 1, High Speed Flow, Oxford University Press, 1953

[8]Bowcutt, Kevin G., "Optimization of hypersonic Waveriders Derived from Cone Flows Including Viscous Effects", Ph.D. Dissertation, Department of Aerospace Engineering, University of Maryland, College Park, Maryland, 1986

[9]Hilerath, J., " Tables of Thermal Properties of Gases", National Bureau of Standards Circular 564, November 1955

[10]McLaughlin, Thomas A., "Viscous Optimized Hypersonic Waveriders for chemical Equilibrium Flow", M.S. Thesis, Department of Aerospace Engineering, University of Maryland, College Park, Maryland, 1990, UM-AERO-90-17.

[11]Anonymous, "U.S. Standard Atmosphere", 1976, U.S. Government Printing Office, Washington D.C., Oct. 1976.

[12]NASA Glenn Research Center,
URL:http://www.grc.nasa.gov/WWW/K-12/airplane/atmosmet.html, Feb.15, 2005.

[13]William H. Heiser, David T. Pratt "Hypersonic Airbreathing Propulsion." AIAA Education Series. ISBN: 1-56347-035-7, Published by American Institute of Aeronautics and Astronautics. Inc 1994.

[14]Kuchemann, D. "The Aerodynamic Design of Aircarft", Pergamon Press, New York, 1978.